

Ultrafast transport-mediated homogenization of photoexcited electrons governs the softening of the A_{1g} phonon in bismuth

F. Thiemann ^{1,*}, G. Sciaini ², A. Kassen,¹ U. Hagemann ^{3,4}, F. Meyer zu Heringdorf ^{1,3,4} and M. Horn-von Hoegen ^{1,4}

¹*Department of Physics, University of Duisburg-Essen, Lotharstrasse 1, 47057 Duisburg, Germany*

²*The Ultrafast Electron Imaging Lab, Department of Chemistry, and Waterloo Institute for Nanotechnology, University of Waterloo, Waterloo, Ontario, Canada N2L 3G1*

³*Interdisciplinary Center for Analytics on the Nanoscale (ICAN), University of Duisburg-Essen, Carl-Benz-Straße 199, 47057 Duisburg, Germany*

⁴*Center for Nanointegration (CENIDE), University of Duisburg-Essen, Carl-Benz-Straße 199, 47057 Duisburg, Germany*



(Received 5 May 2022; accepted 13 July 2022; published 29 July 2022)

In order to determine the role of nonthermal transport of hot carriers, which is decisive for the dissipation of energy in condensed matter, we performed time-resolved broadband femtosecond transient reflectivity measurements on 7–197-nm-thick Bi(111) films epitaxially grown on Si(111). We monitored the behavior of the Fourier amplitude and the central frequency of the coherent A_{1g} phonon mode as a function of the incident fluence, film thickness, and probe wavelength in the range 580–700 nm. The frequency redshift that follows photoexcitation was used as a robust quantity to determine the effective distribution of excited carriers that governs the dispersive excitation mechanism of coherent A_{1g} phonons in Bi. For Bi films up to 50 nm thickness a homogeneous excitation due to the ultrafast transport of hot charge carriers is observed, limited by a carrier penetration depth of 60 nm independent of the totally deposited laser energy.

DOI: [10.1103/PhysRevB.106.014315](https://doi.org/10.1103/PhysRevB.106.014315)

Bismuth as a Peierls-Jones distorted semimetal [1] with its low equilibrium carrier density and its low effective masses is prone to carrier-induced structural instabilities. One of them is the distinct dispersive excitation of coherent A_{1g} optical phonons which has turned bismuth into one of the most studied materials by ultrafast time-resolved pump-probe techniques [2–14]. Upon photoexcitation the charge carrier density can be transiently increased by orders of magnitude thus drastically changing the potential energy surface (PES) of the atoms [9,10,15]. In the case of bismuth the PES experiences a shift in the minimum that results in the initial coherent displacement of the atoms, launching the A_{1g} phonon mode. With growing density of excited carriers the displacement amplitude of the A_{1g} phonon increases [10,15] as the mode significantly softens [4,16]. In turn, the atomic displacement through the A_{1g} phonon strongly modulates the dielectric properties [17] of the material enabling its observation via femtosecond transient reflectivity (fs-TR) measurements [2–8]. This unique correlation between the density of photoexcited electrons and the behavior of the coherent A_{1g} phonon mode provides a quantity to explore the ultrafast spatial redistribution of excited carriers.

Most fs-TR studies of Bi have focused on the investigation of the dynamics of coherent A_{1g} phonons in either bulk single-crystalline samples or relatively thick Bi films of more than 100 nm at a wide range of excitation conditions [4,6,8,16,18] and temperatures [18–20]. Recent attention has been attracted by studies of coherent A_{1g} phonons in ultrathin

films [6,7,21,22]. Among them, Shin *et al.* [6] performed detailed fs-TR experiments on Bi films with thicknesses down to 25 nm on glass and Si substrates. They concluded that confinement yields a significantly higher density of excited carriers, resulting in increased mode softening and faster dephasing. Studies on bulk samples by Johnson *et al.* [23] and Boschetto *et al.* [24] already indicated the existence of hot carrier transport that later became relevant in thin films [22]. Moreover, in a very recent study of Bi films grown on NaCl(001) single-crystalline substrates, Jnawali *et al.* [22] were able to explore the effects of hot carrier transport and empirically determine the effective hot carrier penetration depth that governs the amplitude of the coherent A_{1g} phonon. However, their use of a single-color probe in the limit of low carrier excitation limited the general applicability of this carrier transport model.

Within fs-TR techniques, the flexibility to control the pump and probe central wavelengths has been essential to provide detailed insights into the nature of the generation mechanism of A_1 phonons [17,25] and reveal the role of stimulated Raman scattering in such a process. A step ahead in spectrally resolved probing is the implementation of ultrashort broadband (or supercontinuum) white light pulses. They enable broad spectral detection and the observation of spectroscopic effects that are not evident when single- or two-color fs-TR measurements are employed due to, e.g., thin film interference effects or absorption minima and maxima arising from critical points in the dielectric function [26].

In this paper we implemented broadband fs-TR (bb-fs-TR) to determine the influence of ultrafast transport on redistribution of excited carriers in epitaxially grown Bi films of

*fabian.thiemann@uni-due.de

different thicknesses and its effect on softening of the coherent A_{1g} phonon. Our experiments reveal a rather complex spectroscopic behavior in the bb-fs-TR spectra as a function of film thickness d and incident pump fluence F . A detailed analysis of the redshift (Δf_c) of the A_{1g} phonon central frequency f_c was performed. The results show that Δf_c is the ideal quantity to determine the degree of excitation and the distribution of excited carriers. The effective hot carrier penetration depth d_{eff} was estimated from measurements in the thin film limit ($d < d_{\text{eff}}$) where the density of excited carriers n can be considered constant across the entire film. We observe that hot carrier transport happens within 150 fs, which corresponds to half an oscillation period of the A_{1g} phonon and could be attributed to either ballistic or diffusive processes [27–32].

Our bb-fs-TR setup is driven by an amplified Ti:sapphire laser with a pulse energy of 1 mJ and a repetition rate of 5 kHz that delivers 160-fs pump pulses centered at a photon wavelength of 800 nm. Relative transient reflectivity changes ($\Delta R/R_0$) originating from variations in electron and hole populations, hot carrier energy relaxation processes, and coherent phonon oscillations were probed by time-delayed supercontinuum white light pulses and detected in a synchronized dispersive spectrometer, which provided a spectrum that spanned from $\lambda_{\text{probe}} \approx 580$ nm to $\lambda_{\text{probe}} \approx 700$ nm. The principle of our setup follows those of others employing the well-established bb-fs-TR method [33]. The supercontinuum was generated by focusing a small fraction of the fundamental beam power ($< 1 \mu\text{J}$) into a 4-mm-thick yttrium aluminum garnet (YAG) crystal. The probed spectral window was limited in the short-wavelength region by the gradually decreasing signal-to-noise ratio and in the long-wavelength limit by a 700-nm short-pass filter placed in front of the spectrometer to block the scattered pump light. A noncollinear arrangement with an angle of 30° between the incident pump and probe beams was used. The full width at half maximum (FWHM) of the pump and probe beam spot sizes at the film's surface was approximately 180 and 130 μm , respectively. The incident pump fluence was varied through the combination of a half-wave plate and a calcite polarizer. The time-resolved bb-fs-TR spectra [$\Delta R/R_0(t, \lambda_{\text{probe}})$] were recorded by periodically blocking the pump beam with a mechanical chopper at 25 Hz and through an optical time delay. The typical time step was 25 fs.

Epitaxial, [111]-oriented Bi films of various nominal thicknesses (10, 20, 30, 40, 50, and 200 nm) were grown on Si(111) substrates as described in Refs. [34,35] using a commercial electron beam evaporator. The crystallinity of the films was verified *in situ* using low-energy electron diffraction (LEED; see Supplemental Material [36]). The Bi film thickness was monitored during deposition using a quartz balance that was calibrated by profilometry and atomic force microscopy to the thickness of reference samples. The equilibrium A_{1g} frequencies in the films were measured employing Raman spectroscopy. Due to the exposure to ambient conditions the nominal values of the film thickness were corrected by subtracting the approximately 3-nm-thick layer of bismuth oxide determined by x-ray diffraction and x-ray reflection [35]. Therefore the effective Bi thicknesses d in our experiments were (7 ± 1) , (17 ± 2) , (27 ± 3) , (37 ± 3) , (47 ± 4) , and (197 ± 11) nm.

The $\Delta R/R_0(t)$ spectrum obtained for the 27-nm-thick Bi film at $F = 0.52 \text{ mJ/cm}^2$ is depicted in Fig. 1(a). Note that in the range $\lambda_{\text{probe}} \approx 640\text{--}680$ nm (between the dashed lines), the amplitude of the oscillation flips its sign, i.e., suffers a relative π -phase shift. The two sinusoidal traces in Fig. 1(a) are placed as a guide for the eye and illustrate that the initial oscillation amplitude is negative below 640 nm and positive above 680 nm. The marked area at (650.0 ± 1.5) nm (ten pixels in the spectrometer) in Fig. 1(a) illustrates the spectral range of averaging for the traces shown in Fig. 1(b). Ultimately, the sign flip of $\Delta R/R_0$ in Fig. 1(a) leads to a phase node or nonoscillatory signal in the time domain at $\lambda_{\text{probe}} \approx 650$ nm as seen in the corresponding trace for $d = 27$ nm in Fig. 1(b). This renders any analysis based on the direct comparison of phonon oscillation amplitudes at a single probe wavelength near $\lambda_{\text{probe}} \approx 650$ nm very challenging, highlighting the advantages of broadband over single-color probes [26].

Therefore we employed fast Fourier transformation (FFT) in order to unambiguously obtain the frequency f , proportional to the degree of excitation, from the $\Delta R/R_0(t)$ spectra. Figure 1(c) shows the Fourier spectrum obtained from the data shown in Fig. 1(a). We employed the time-derivative method to remove the slowly varying background signal arising from changes in the electronic population. This method provides the oscillatory residuals necessary to extract f at each λ_{probe} via FFTs without the need to fit the temporal traces. The spectral region affected by the phase node $\lambda_{\text{probe}} \approx 640\text{--}680$ nm is now clearly visible as a zone where the FFT amplitude of the coherent A_{1g} phonon is approximately zero. Note that the actual coherent A_{1g} phonon displacement modulates the dielectric properties of the material with the same frequency f across the probed spectral window. Therefore we averaged the FFT spectra along λ_{probe} to obtain the average Fourier transform (FT) spectrum (white trace) with the frequency at maximum $f_c \approx 2.8$ THz. Figure 1(d) displays the average FT spectra for $d = 27$ nm as well as the values of f_c obtained for $d = 17$ nm, $d = 27$ nm, and $d = 197$ nm as a function of F . The f_c are compared with the measured Raman frequency f_{Raman} (dashed line) for the thickest film, which can be considered as a bulk reference. f_{Raman} reflects the frequency f_0 of the A_{1g} mode without excitation. This analysis procedure was carried out for all samples, and the resulting frequencies f_c and frequency changes $\Delta f_c = f_c - f_0$ are shown in Figs. 1(d) and 2(a), respectively.

We observe an almost linear redshift in f_c upon increasing F , as predicted by experiment [16] and theory [15]. Furthermore, the frequencies of the A_{1g} mode for films with different thicknesses d shown in Fig. 1(d) exhibit a pronounced difference in their fluence dependency. Since the frequency change Δf_c depends on the number of excited carriers [10,15], we assumed that Δf_c can be used as the quantity that determines the effective degree of excitation of the film. Therefore we relate it to the density of excited carriers $n(z)$ after hot carrier transport and thermalization or absorbed energy per unit volume $\rho(z) \propto n(z)$, which depends in general on the propagation distance from the film's surface (z). More specifically, if it is assumed that carrier multiplication after absorption always results in the same number of excited carriers per photon, $\rho(z)$ should refer to the spatial distribution of the excited carriers. The term “hot carrier density” describes the initial distribution of

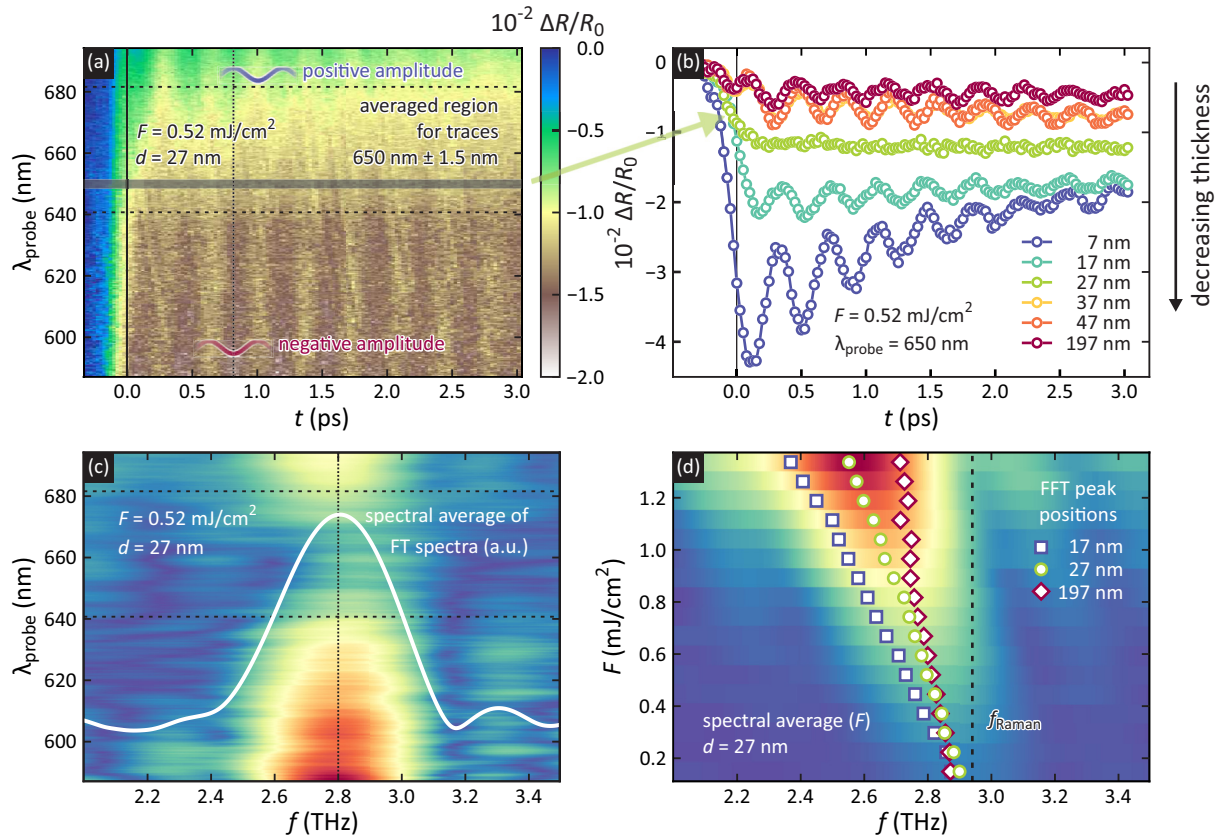


FIG. 1. (a) Time-resolved bb-fs-TR spectrum obtained for the 27-nm-thick Bi film. The sinusoidal traces are a guide for the eye. (b) Temporal traces obtained for all films at $\lambda_{\text{probe}} = 650$ nm after averaging along a bin of 3 nm in width as depicted in (a) for $d = 27$ nm. (c) Fourier power spectrum obtained from the analysis of the bb-fs-TR spectrum shown in (a). The white trace represents the spectral average. (d) Spectral averages of the Fourier power spectra for $d = 27$ nm and the peak value for $d = 17$ nm, $d = 27$ nm, and $d = 197$ nm as a function of F compared with the Raman frequency (dashed line) of the 197-nm-thick film, serving as a bulk reference.

charge carriers immediately after excitation, whereas “density of excited carriers” refers to the distribution of carriers after transport and thermalization.

The two extreme scenarios one would expect for $\rho(z)$ are (i) a complete homogeneous distribution of excited carriers n_{hom} across the entire film thickness characterized by a constant absorbed energy density ρ_{hom} or (ii) a distribution of excited carriers that follows the spatial distribution of the originally absorbed pump light. The distribution of $\rho(z)$ normalized by the initially absorbed energy density ρ_0 at the surface is sketched for scenario (ii) as case A in Fig. 2(c) and for scenario (i) as cases B and C in Figs. 2(d) and 2(e). The exemplary time stamps in Figs. 2(c)–2(e) emphasize that scenario (ii) is the initial distribution of hot carriers within the first few femtoseconds for cases B and C as well. In order to quantify the redshift Δf_c and compare it with scenarios (i) and (ii), we describe it with a linear slope α , and thus

$$f_c(F_{\text{abs}}) = f_0 - \Delta f_c = f_0 - \alpha F_{\text{abs}}. \quad (1)$$

We fitted Eq. (1) to the measured f_c for each film as shown by the solid lines in Fig. 2(a). We found that α gradually increases with decreasing film thickness. The data points in diluted colors shown in Fig. 2(a) are excluded from fitting due to radiation damage of the film ($d = 7$ nm) and deviation from the linear behavior ($d = 197$ nm). A possible explanation for

this deviation may be an increased hot carrier penetration depth. Radiation damage was confirmed by rendering the recovery of low-fluence results impossible after exceeding the threshold of $F_{\text{abs}} \approx 0.8$ mJ/cm². Here, f_0 is the extrapolated value of f_c at $F_{\text{abs}} = 0$ for a given d . Unfortunately, due to uncertainties in the fluence the error in f_0 is quite large. This is why we used the frequency shift Δf_c and not the plain frequency f_c as the relevant quantity. However, we still need to ensure that differences in f_0 are significantly smaller than the observed redshift. Therefore we performed Raman spectroscopy to determine the frequency $f_0 \approx f_{\text{Raman}}$ of the A_{1g} mode without any carrier-induced redshifts. f_{Raman} as a function of d is shown in the inset in Fig. 2(a). A clear blueshift in f_{Raman} towards thinner films is visible. This blueshift is likely induced by compressive strain, which is expected for Bi/Si(111) films, as studied by Payer *et al.* [35]. Yet this blueshift is negligible compared with the pronounced redshift Δf_c . F_{abs} is the absorbed fluence that accounts for losses by reflection at the surface and transmission into the substrate as well as gains in absorption by reflection at the film/substrate interface, which all was calculated employing the transfer matrix method (TMM) [37,38]. The ratio between F_{abs} and F as a function of d is shown in Fig. 2(f). The optical losses at the interface are illustrated by the difference of $F_{\text{abs}}(d)$ (solid line) and $\lim_{d \rightarrow \infty} F_{\text{abs}}(d)$ (dotted line) in Fig. 2(f). We

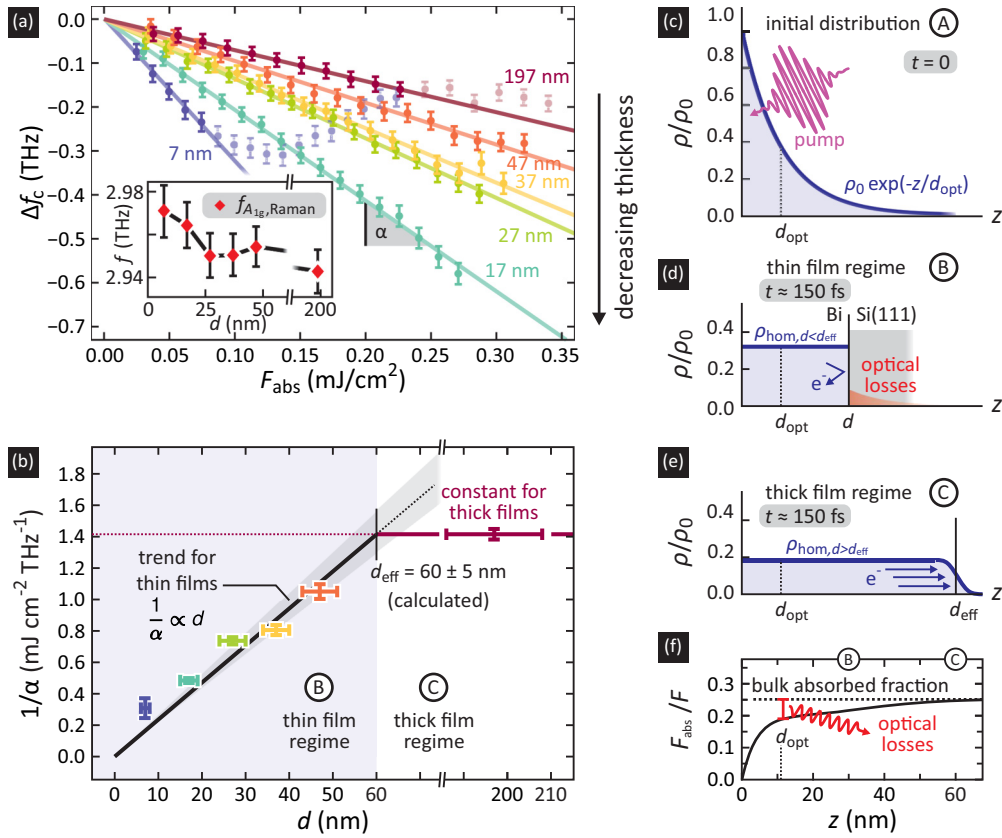


FIG. 2. (a) Frequency shift $\Delta f_c = f_c - f_0$ of the A_{1g} mode as a function of F_{abs} for films of different thickness. The solid lines represent the slopes of the linear fit $f_c = f_0 - \alpha F_{\text{abs}}$. The inset shows the equilibrium frequency of the A_{1g} mode $f_{\text{Raman}} \approx f_0$ obtained from Raman spectroscopy as a function of film thickness d . (b) Inverse slope $1/\alpha$ from (a) as a function of d . The thin film regime (case B) is represented by a linear trend (black line), and the $d = 197$ nm value serves as a bulk reference (horizontal line) in the thick film regime (case C). The intersection of both determines the effective hot carrier penetration depth $d_{\text{eff}} = 60$ nm. The standard deviation of the trend's linear fit is marked by the gray area. (c) Distribution of energy in the carrier system within the first few femtoseconds (case A) after excitation, represented by the absorbed energy density $\rho(z) = \rho_0 \exp(-z/d_{\text{opt}})$, whereas d_{opt} is the calculated optical penetration depth. (d) and (e) show the homogeneous distribution of $\rho(z)$ for the thin film (case B) and thick film (case C) regime at later times. (f) Calculated ratio of absorbed fluence F_{abs} over incident fluence F .

safely assume that there are no losses of energy by carrier transport to the substrate due to the formation of a Schottky barrier at the Bi/Si(111) interface [39]. In the first case of a homogenous excited carrier distribution [scenario (i)], Δf_c as a function of F_{abs} follows

$$\Delta f_c \propto n_{\text{hom}} \propto \rho_{\text{hom}} = \frac{F_{\text{abs}}}{d}. \quad (2)$$

This inverse proportionality of Δf_c and ρ_{hom} on d results in the drastically increased slope α [see Eq. (1)] towards thin films. The dramatic impact of inverse proportionality is shown in Figs. 2(d) and 2(e), comparing ρ_{hom} for two different film thicknesses excited with the same arbitrary F . The areas underneath the curves in Figs. 2(d) and 2(e) are approximately the same as in the initial distribution in Fig. 2(c), and this reflects the totally absorbed energy in the film.

We will show that in the thin film limit our observations can be well described by the first scenario [scenario (i)], but we still need to rule out the second one [scenario (ii)], especially because scenario (ii) describes the initial distribution of hot carriers as well, before the carrier transport trans-

forms the initial distribution into a homogeneous distribution of excited carriers [scenario (i)]. For the second scenario, i.e., ignoring hot carrier transport, carrier multiplication, and thus their effects on the A_{1g} vibrational coherence, $\rho(z)$ will follow the Beer-Lambert law for light absorption, $\rho(z) = \rho_0 \exp(-z/d_{\text{opt}})$ [see Fig. 2(c)]. For thin films we include corrections to account for the transmission and reflection of the pump field at the Bi/Si interface. We have calculated the optical penetration depth $d_{\text{opt}} = 11$ nm for $\lambda = 800$ nm using the dielectric function of Bi measured by Toudert *et al.* [40] and found that thin film corrections to the value of ρ_0 are only within 8% for the thinnest film. Considering that optical reflectivity essentially probes the surface of the film, the observed A_{1g} phonon frequency f_c should be then proportional to the absorbed energy density at the surface ρ_0 , which is still proportional to the fluence F , but nearly independent of the film thickness d . Thus the expected values for $f_c(F)$ should be almost identical for all films. This is, however, not the case as shown by the varying redshifts for different d in Fig. 1(d). The redshift is about three times more pronounced in the 17-nm-thick film than in the 197-nm-thick film. Therefore

we render scenario (ii) as incorrect and continue with the first scenario [scenario (i)]. Previously, we have described scenario (i) as a homogeneous distribution $\rho(z) = \rho_{\text{hom}}$ across the entire film thickness. Since bulk samples show demonstrably still significant redshifts in the A_{1g} mode, the transport of carriers has to stop at some distance while increasing the film thickness. To resolve this issue, we introduce the thin and thick film regimes. In the former the transport of carriers is limited by the film thickness d [see Fig. 2(d)], and for the latter [see Fig. 2(e)] we introduce the limiting effective hot carrier penetration depth d_{eff} . Note that the edge of $\rho(z)$ is sharp in Fig. 2(d) and smeared out in Fig. 2(e) due to the missing Schottky barrier in the thick film regime. In the thin film regime the combination of Eqs. (1) and (2) yields the following relationship: $1/\alpha \propto d$. As shown in Fig. 2(b) the five thinnest samples exhibit the relation $1/\alpha \propto d$ and are within the thin film limit. We carried out a procedure similar to that presented by Jnawali *et al.* [22] and determined $d_{\text{eff}} = (60 \pm 5)$ nm from the intersection of the thin film regime's linear trend (black line) with the bulk's limit value (horizontal line, $d = 197$ nm). This limit value cannot be exceeded, since bulk samples should exhibit the broadest spread of excited carriers.

We found that our d_{eff} is larger than the one found by Jnawali *et al.* [22]. A plausible explanation is a missing annealing step during growth of the Bi/NaCl(001) samples used by Jnawali *et al.*, as described in their growth method originally published by Payer *et al.* [41]. Annealing is a common method for defect reduction. Thus, in the case of Bi/NaCl(001) an increased number of lattice defects remain in the Bi film. Since the electron mean free path is expected to depend on the sample quality (crystallinity, impurities, dislocations, etc.), the annealed films used in our study should exhibit a larger d_{eff} .

Furthermore, we can conclude that the transport behavior in the thin film regime and effective hot carrier penetration depth d_{eff} are, within the measured range of fluences F , independent of the totally deposited energy. If the process of homogenization would be distorted, the ratios between Δf_c for different d would change as a function of F_{abs} . For the behavior of d_{eff} , two simple cases to discuss are a decreasing or increasing d_{eff} as a function of F_{abs} . The first results in a larger $|\Delta f_c|$ for $d = 197$ nm and eventually for $d = 47$ nm, etc., whereas the latter results in a declining $|\Delta f_c|$ for $d = 197$ nm. The latter case can be applied to some of the last six data points ($F_{\text{abs}} > 0.22$ mJ/cm²) shown in diluted colors in Fig. 2(a). However, since they are scattered and show no clear trend, one has to be very careful concluding that there is a modification of d_{eff} . Therefore hot carrier transport at higher excitation levels than the presented ones requires further attention.

Concerning the nature of the hot carrier transport process, which may be diffusive as proposed by Johnson *et al.* [23],

ballistic as discussed by Brorson *et al.* [42] and Suárez *et al.* [43], or likely a combination of both, we are unable to give an answer. Due to the temporal response function of our pump-probe setup (≈ 160 fs) we cannot differentiate between these two possible contributions. Such hot carrier transport mechanisms have been investigated recently by time-resolved microscopy in metals and semiconductors by Block *et al.* [31] and Sung *et al.* [32], respectively. Those results show that not only are the differences in propagation velocity important but also the time dependency of the mean-square displacement of hot carriers is the deciding parameter for the transport mechanism. In our temporal traces the frequency redshifts are visible after half an oscillation period of the A_{1g} phonon's mode. At this point, no changes in the instantaneous frequency, which would be an indication for a slower hot carrier transport, are observed. This was verified through short-time FT (see Supplemental Material [36]). We thus conclude that the spread of hot carriers occurs on a timescale shorter than 150 fs, i.e., shorter than half an oscillation period of the A_{1g} vibrational coherence; that is, the carriers propagate with a velocity comparable to the Fermi velocity of bismuth.

In conclusion, we demonstrated a simple and improved approach to determine the effective hot carrier penetration depth, the excited carrier distribution, and their fluence dependency in Bi, which behavior is found to be independent of the totally deposited energy. Here, we employed the detected redshift of the A_{1g} mode to determine the absorbed energy density ρ proportional to the density of excited carriers n . In contrast to the amplitude of the oscillatory component in $\Delta R/R_0(t)$ the change in frequency is not affected by thin film interference effects or absorption minima or maxima arising from critical points in the dielectric function. This allowed us to conclude that the hot carriers are distributed homogeneously throughout thin films ($d < 60$ nm) on a timescale of less than 150 fs. These findings will allow the further study and characterization of ultrafast hot carrier transport and its manipulation, e.g., by defects and impurities, not only in bismuth but also in other materials.

We gratefully acknowledge fruitful discussions with R. Merlin and A. von Hoegen. Funding by the Deutsche Forschungsgemeinschaft (DFG, German Research Foundation) through project B04 of Collaborative Research Center SFB 1242 "Nonequilibrium dynamics of condensed matter in the time domain" (Project No. 278162697) is appreciated. G.S. acknowledges the support of the National Science and Engineering Research Council of Canada, the Ontario Early Researcher Award program, the Canada Foundation for Innovation, and the Canada Research Chair program.

The authors declare no competing financial interest.

- [1] R. Peierls, *More Surprises in Theoretical Physics* (Princeton University Press, Princeton, 1991).
- [2] T. K. Cheng, S. D. Brorson, A. S. Kazeroonian, J. S. Moodera, G. Dresselhaus, M. S. Dresselhaus, and E. P. Ippen, Impulsive excitation of coherent phonons observed in reflection in bismuth and antimony, *Appl. Phys. Lett.* **57**, 1004 (1990).

- [3] M. Hase, K. Mizoguchi, H. Harima, S. Nakashima, M. Tani, K. Sakai, and M. Hangyo, Optical control of coherent optical phonons in bismuth films, *Appl. Phys. Lett.* **69**, 2474 (1996).
- [4] M. F. DeCamp, D. A. Reis, P. H. Bucksbaum, and R. Merlin, Dynamics and coherent control of high-amplitude optical phonons in bismuth, *Phys. Rev. B* **64**, 092301 (2001).

- [5] D. Boschetto, E. G. Gamaly, A. V. Rode, B. Luther-Davies, D. Glijer, T. Garl, O. Albert, A. Rousse, and J. Etchepare, Small Atomic Displacements Recorded in Bismuth by the Optical Reflectivity of Femtosecond Laser-Pulse Excitations, *Phys. Rev. Lett.* **100**, 027404 (2008).
- [6] T. Shin, J. W. Wolfson, S. W. Teitelbaum, M. Kandyla, and K. A. Nelson, Carrier confinement and bond softening in photoexcited bismuth films, *Phys. Rev. B* **92**, 184302 (2015).
- [7] K. Ishioka, M. Kitajima, O. V. Misochko, and T. Nagao, Ultrafast phonon dynamics of epitaxial atomic layers of Bi on Si(111), *Phys. Rev. B* **91**, 125431 (2015).
- [8] S. W. Teitelbaum, T. Shin, J. W. Wolfson, Y.-H. Cheng, I. J. Porter, M. Kandyla, and K. A. Nelson, Real-Time Observation of a Coherent Lattice Transformation into a High-Symmetry Phase, *Phys. Rev. X* **8**, 031081 (2018).
- [9] K. Sokolowski-Tinten, C. Blome, J. Blums, A. Cavalleri, C. Dietrich, A. Tarasevitch, I. Uschmann, E. Förster, M. Kammler, M. Horn-von Hoegen, and D. von der Linde, Femtosecond x-ray measurement of coherent lattice vibrations near the Lindemann stability limit, *Nature (London)* **422**, 287 (2003).
- [10] D. M. Fritz, D. A. Reis, B. Adams, R. A. Akre, J. Arthur, C. Blome, P. H. Bucksbaum, A. L. Cavalieri, S. Engemann, S. Fahy, R. W. Falcone, P. H. Fuoss, K. J. Gaffney, M. J. George, J. Hajdu, M. P. Hertlein, P. B. Hillyard, M. Horn-von Hoegen, M. Kammler, J. Kaspar *et al.*, Ultrafast bond softening in bismuth: Mapping a solid's interatomic potential with x-rays, *Science* **315**, 633 (2007).
- [11] G. Sciaini, M. Harb, S. G. Kruglik, T. Payer, C. T. Hebeisen, F.-J. M. zu Heringdorf, M. Yamaguchi, M. Horn-von Hoegen, R. Ernstorfer, and R. J. D. Miller, Electronic acceleration of atomic motions and disordering in bismuth, *Nature (London)* **458**, 56 (2009).
- [12] S. L. Johnson, P. Beaud, E. Vorobeva, C. J. Milne, É. D. Murray, S. Fahy, and G. Ingold, Directly Observing Squeezed Phonon States with Femtosecond X-Ray Diffraction, *Phys. Rev. Lett.* **102**, 175503 (2009).
- [13] K. Sokolowski-Tinten, R. K. Li, A. H. Reid, S. P. Weathersby, F. Quirin, T. Chase, R. Coffee, J. Corbett, A. Fry, N. Hartmann, C. Hast, R. Hettel, M. Horn-von Hoegen, D. Janoschka, J. R. Lewandowski, M. Ligges, F. M. zu Heringdorf, X. Shen, T. Vecchione, C. Witt *et al.*, Thickness-dependent electron–lattice equilibration in laser-excited thin bismuth films, *New J. Phys.* **17**, 113047 (2015).
- [14] F. Qi, Z. Ma, L. Zhao, Y. Cheng, W. Jiang, C. Lu, T. Jiang, D. Qian, Z. Wang, W. Zhang, P. Zhu, X. Zou, W. Wan, D. Xiang, and J. Zhang, Breaking 50 Femtosecond Resolution Barrier in MeV Ultrafast Electron Diffraction with a Double Bend Achromat Compressor, *Phys. Rev. Lett.* **124**, 134803 (2020).
- [15] É. D. Murray, D. M. Fritz, J. K. Wahlstrand, S. Fahy, and D. A. Reis, Effect of lattice anharmonicity on high-amplitude phonon dynamics in photoexcited bismuth, *Phys. Rev. B* **72**, 060301(R) (2005).
- [16] M. Hase, M. Kitajima, S. I. Nakashima, and K. Mizoguchi, Dynamics of Coherent Anharmonic Phonons in Bismuth Using High Density Photoexcitation, *Phys. Rev. Lett.* **88**, 067401 (2002).
- [17] T. Stevens, J. Hebling, J. Kuhl, and R. Merlin, Coherent phonon dynamics studied by impulsive stimulated Raman scattering, *Phys. Status Solidi (b)* **215**, 81 (1999).
- [18] T. Garl, E. G. Gamaly, D. Boschetto, A. V. Rode, B. Luther-Davies, and A. Rousse, Birth and decay of coherent optical phonons in femtosecond-laser-excited bismuth, *Phys. Rev. B* **78**, 134302 (2008).
- [19] M. Hase, K. Mizoguchi, H. Harima, S. I. Nakashima, and K. Sakai, Dynamics of coherent phonons in bismuth generated by ultrashort laser pulses, *Phys. Rev. B* **58**, 5448 (1998).
- [20] K. Ishioka, M. Kitajima, and O. V. Misochko, Temperature dependence of coherent A_{1g} and E_g phonons of bismuth, *J. Appl. Phys.* **100**, 093501 (2006).
- [21] F. He, E. S. Walker, Y. Zhou, R. D. Montano, S. R. Bank, and Y. Wang, Phase transition in epitaxial bismuth nanofilms, *Appl. Phys. Lett.* **117**, 073103 (2020).
- [22] G. Jnawali, D. Boschetto, L. M. Malard, T. F. Heinz, G. Sciaini, F. Thiemann, T. Payer, L. Kremeyer, F.-J. M. zu Heringdorf, and M. Horn-von Hoegen, Hot carrier transport limits the dispersive excitation of coherent phonons in bismuth, *Appl. Phys. Lett.* **119**, 091601 (2021).
- [23] S. L. Johnson, P. Beaud, C. J. Milne, F. S. Krasniqi, E. S. Zijlstra, M. E. Garcia, M. Kaiser, D. Grolimund, R. Abela, and G. Ingold, Nanoscale Depth-Resolved Coherent Femtosecond Motion in Laser-Excited Bismuth, *Phys. Rev. Lett.* **100**, 155501 (2008).
- [24] D. Boschetto, T. Garl, and A. Rousse, Ultrafast dielectric function dynamics in bismuth, *J. Mod. Opt.* **57**, 953 (2010).
- [25] T. E. Stevens, J. Kuhl, and R. Merlin, Coherent phonon generation and the two stimulated Raman tensors, *Phys. Rev. B* **65**, 144304 (2002).
- [26] M. Cheng, S. Zhong, N. Rivas, T. Dekker, A. A. Petruk, P. Gicala, K. Pichugin, F. Chen, X. Luo, Y. Sun, A. W. Tsun, and G. Sciaini, Photoinduced interlayer dynamics in T_d -MoTe₂: A broadband pump-probe study, *Appl. Phys. Lett.* **120**, 123102 (2022).
- [27] J. Hayes and A. Levi, Dynamics of extreme nonequilibrium electron transport in GaAs, *IEEE J. Quantum Electron.* **22**, 1744 (1986).
- [28] V. E. Gusev and O. B. Wright, Ultrafast nonequilibrium dynamics of electrons in metals, *Phys. Rev. B* **57**, 2878 (1998).
- [29] O. B. Wright, B. Perrin, O. Matsuda, and V. E. Gusev, Ultrafast carrier diffusion in gallium arsenide probed with picosecond acoustic pulses, *Phys. Rev. B* **64**, 081202(R) (2001).
- [30] M. Hada, D. Zhang, A. Casandruc, R. J. D. Miller, Y. Hontani, J. Matsuo, R. E. Marvel, and R. F. Haglund, Hot electron injection driven phase transitions, *Phys. Rev. B* **86**, 134101 (2012).
- [31] A. Block, M. Liebel, R. Yu, M. Spector, Y. Sivan, F. J. G. de Abajo, and N. F. van Hulst, Tracking ultrafast hot-electron diffusion in space and time by ultrafast thermomodulation microscopy, *Sci. Adv.* **5**, eaav8965 (2019).
- [32] J. Sung, C. Schnedermann, L. Ni, A. Sadhanala, R. Y. S. Chen, C. Cho, L. Priest, J. M. Lim, H.-K. Kim, B. Monserrat, P. Kukura, and A. Rao, Long-range ballistic propagation of carriers in methylammonium lead iodide perovskite thin films, *Nat. Phys.* **16**, 171 (2020).
- [33] S. A. Kovalenko, A. L. Dobryakov, J. Ruthmann, and N. P. Ernsting, Femtosecond spectroscopy of condensed phases with chirped supercontinuum probing, *Phys. Rev. A* **59**, 2369 (1999).
- [34] M. Kammler and M. Horn-von Hoegen, Low energy electron diffraction of epitaxial growth of bismuth on Si(111), *Surf. Sci.* **576**, 56 (2005).

- [35] T. Payer, C. Klein, M. Acet, V. Ney, M. Kammler, F.-J. M. zu Heringdorf, and M. Horn-von Hoegen, High-quality epitaxial Bi(111) films on Si(111) by isochronal annealing, *Thin Solid Films* **520**, 6905 (2012).
- [36] See Supplemental Material at <http://link.aps.org/supplemental/10.1103/PhysRevB.106.014315> for additional information on sample growth and an example of short-time Fourier transformation spectrograms.
- [37] J. S. C. Prentice, Coherent, partially coherent and incoherent light absorption in thin-film multilayer structures, *J. Phys. D: Appl. Phys.* **33**, 3139 (2000).
- [38] C. C. Katsidis and D. I. Siapkas, General transfer-matrix method for optical multilayer systems with coherent, partially coherent, and incoherent interference, *Appl. Opt.* **41**, 3978 (2002).
- [39] K. Hricovini, G. L. Lay, A. Kahn, A. Taleb-Ibrahimi, and J. Bonnet, Initial stages of Schottky-barrier formation of Bi/Si(111) and Bi/Si(100) interfaces, *Appl. Surf. Sci.* **56–58**, 259 (1992).
- [40] J. Toudert, R. Serna, I. Camps, J. Wojcik, P. Mascher, E. Rebollar, and T. A. Ezquerro, Unveiling the far infrared-to-ultraviolet optical properties of bismuth for applications in plasmonics and nanophotonics, *J. Phys. Chem. C* **121**, 3511 (2017).
- [41] T. Payer, I. Rajković, M. Ligges, D. von der Linde, M. Horn-von Hoegen, and F.-J. Meyer zu Heringdorf, Ultrathin epitaxially grown bismuth (111) membranes, *Appl. Phys. Lett.* **93**, 093102 (2008).
- [42] S. D. Brorson, J. G. Fujimoto, and E. P. Ippen, Femtosecond Electronic Heat-Transport Dynamics in Thin Gold Films, *Phys. Rev. Lett.* **59**, 1962 (1987).
- [43] C. Suárez, W. E. Bron, and T. Juhasz, Dynamics and Transport of Electronic Carriers in Thin Gold Films, *Phys. Rev. Lett.* **75**, 4536 (1995).